Colloid and Surface Science
2021; 6(1): 8-15
http://www.sciencepublishinggroup.com/j/css
doi: 10.11648/j.css.20210601.12
ISSN: 2578-9120 (Print); ISSN: 2578-9236 (Online)

A Displacement-energy Model Approach for Evaluating the Interfacial Stress in Multilayer Film Structures Based on the Interactions of Grains at the Interface

Stephen Ogbonna Mbam

Department of Mechanical/Mechatronic Engineering, Alex Ekwueme Federal University, Ndufu-Alike Ikwo, Abakaliki, Nigeria

Email address:
ogbonna.mbam@funai.edu.ng

To cite this article:
Stephen Ogbonna Mbam. A Displacement-energy Model Approach for Evaluating the Interfacial Stress in Multilayer Film Structures Based on the Interactions of Grains at the Interface. *Colloid and Surface Science*. Vol. 6, No. 1, 2021, pp. 8-15. doi: 10.11648/j.css.20210601.12

Received: September 25, 2021; **Accepted**: October 22, 2021; **Published**: November 24, 2021

Abstract: For multilayer film structures, mechanical failure is usually taken place at the interface. To deeply understand the typical issue, it is first essential to know the stress status at the interlayer surface. For this aim, in this work, the author presented displacement-energy models (DEM) for accurately calculating the interfacial stress in multilayer film structures and the impact of the morphology and size of the interacting grains at the interface. The stress-inducing mechanisms are related to the displacement-energy phenomenon of the interacting grains in the structure caused by the deposition technique. In contrast, the interfacial residual stress-evolution in the deposited films is determined from the change in the lattice constant between interacting grains as a function of temperature and time during the deposition and cool-down process. The interacting grains understudied have different morphology with flat and curved surfaces and sizes. Concerning the yttrium barium copper oxide (YBCO) films deposited on the lanthanum aluminum oxide ($LaAlO_3$) substrate, the computed results showed that the morphology and size of the interacting grains affect the net interfacial residual stresses in the YBCO films significantly. Also, the results of the DEM models agree well with the measured value by the X-ray diffraction method (XRD). Specifically, the computed stress in the YBCO films for the interacting grains with spherical surfaces is 0.18 GPa. Similarly, that measured by the XRD method is 0.178± 0.053 GPa. In the future, the findings of this study could be essential in the defect inspection of several Multilayer Engineering Materials, including composites for various applications, which often consist of grains with different morphology and size.

Keywords: Displacement-energy Model (DEM) Approach, Interfacial Stress, Grains Interactions, Yttrium Barium Copper Oxide (YBCO) Crystal

1. Introduction

Recently, a specific review of thin-film coating and projection of its prospects, reported that thin-film structures are very crucial in fast transportation, green energy generation, and rapid communications [1]. For instance, several studies indicated that the magnetic levitation trains (MagLev) consist of high-field magnet coils made of thin-film structures such as rare-earth barium copper oxide (REBCO) coated conductor (CC) wires [2-5]. Also, several studies indicated that the harnessing of solar energy for electricity hugely relies on thin-film solar cells, which are typically thin-film structures [6-8].

Unfortunately, thin-film structures usually suffer high mechanical stresses (residual stresses) [9, 10]. These mechanical stresses are consistent with all thin-film structures for all deposition techniques. The significant presence of residual stresses, especially in multilayered film structures, can cause the interfaces of its layers to degrade. Several valuable experiments had been carried out by Korzeniewska, E, and Szczęsny, A and Xia, W., *et al*., [11, 12] and several models developed by Li, Z-X., *et al*., Mbam, S. O. and Gou, X-F, Sugino, C., *et al*., Cheikh, I. B., *et al*., Mikula, J., *et al*., and Mbam, S. O., *et al*., [13-18] to advance the mastery of the interfacial failure mechanics in the thin-film structures. However, some materials parameters such as the interfacial stress based on the interaction of the grains at the interface are

not clear [19, 20].

The critical review by the author of this work and others indicated that the societal demand and associated challenges of thin-film structures would remain vibrant and active research areas for periods far into the future [1]. Also, the displacement-energy model (DEM) approach showed high fidelity in the determination of the interfacial residual stress distribution and damage-evolution in thin-film structures at the submicron-scale [14]. Unlike the kinetic models developed by Chason, E., *et al*., [20], which could not predict the interfacial stress based on the interactions of the grains, the DEM approach can predict the interfacial stress based on the interactions of the grains with identified morphology and sizes. However, the earlier implementations of the DEM approach considered only the interactions of grains or deposited films that have flat surfaces [14, 18, 21, 22]. In this work, the author extended the DEM approach to predict the interfacial stress in a multilayer film structure based on the interactions of the grains at the interface, consisting of interacting grains with flat and curved surfaces. Also, the author investigated the dependence of the interfacial stress on the grain size of the thin-film structure.

2. The Displacement-energy Model (DEM) Approach

The displacement-energy model (DEM) approach is developed majorly for simulating the static and dynamic mechanical behaviors of interface defects or failure in multilayer thin-film structures at submicron-scale [14, 18]. In a detailed description of the interfacial stress evolution during the deposition of films onto a substrate in the study of Mbam *et al*., [1], the grains of the deposited films consist of cubic, pyramid, pyramid frustum, and spherical shapes. Based on the above system, the interacting surfaces would include flat-flat surface interaction, flat-curved surface interaction, and curved-curved surface interaction. The evolution of the interfacial stress is determined by the displacement function of principal components of the thin-film structure (i.e., films and substrate) induced by the kinetic and thermal energy of the deposited films. First, the kinetic energy of the deposited films and deposition flux gas cause the whole structure to vibrate. Second, the thermal energy of the deposited films and deposition flux gas heats the whole system. In the momentary seizure of deposition particles, the deposited films and substrate would have different eigenfunctions due to their different physical and mechanical properties. Also, on the cool-down of the structure, the deposited films and substrate would shrink at a different rate because of their different coefficient of thermal expansion. These interlayer interactions induce compressive or tensile stress in the deposited films. The induced stresses could emanate from trapping residual gas molecules, lattice mismatch, and microvoids. For this phenomenon, the interfacial stress can graduate from compressive to tensile or vis-a-vis (C-T-C) as a function of time during deposition depending on the interacting energies, surfaces, and grain sizes.

According to the DEM approach described in the earlier study by Mbam, S. O. and Gou, X-F [14], the net interfacial stress in an interface for interacting grains with flat surfaces can be described by

$$\sigma_{\mathrm{j},t(F-F)}^{net} = -\left[\left(\frac{A_{11}}{6\pi(d_i+\Delta d)^3}\right)^{th} + \left(\frac{A_{12}}{6\pi(d_j+\Delta w_{j,t})^3}\right)^{sd} \right], \quad (1)$$

where the subscripts j denote an interface, t refers to time, $F-F$ refers to flat-flat surface interaction between two grains, A_{11} and A_{12} are the Hamaker coefficients described by Mbam, S. O. and Gou, X-F, [23]

$$A_{11} = \pi^2 \rho^2 C_L \text{ and } A_{12} \approx \sqrt{A_{11}A_{22}}, \quad (2)$$

where ρ is the atomic density (number of atoms per unit volume) of the body and C_L (*London constant*) is the coefficient in the atom-atom pair potential (top row). d is the lattice constant, i is a specific grain, Δd is the change in the lattice constant due to the thermal stress mismatch in the grains. Appendix A contains the detailed derivation of Δd using the force and moments balance method. Still, in equation (1), w is the deflection function of a grain, Δw is the change in the lattice constant due to the structural dynamics (vibration) of the grains during deposition processes. One can read the detailed derivation of the Δw in Mbam, S. O. and Gou, X-F and Mbam, S. O., *et al*., [14, 18]. Also, equation (1), *th* and *sd* denotes the thermal and vibration stress, respectively.

For the extension of the DEM phenomenon to predict the interfacial stress in a multilayer film structure consisting of interacting grains with flat and curved surfaces as shown in Figure 1, the net interfacial stress function for flat-curved surface interaction as a function of temperature and time can be described by

$$\sigma_{\mathrm{j},t(\mathrm{F-}C)}^{net} = -\frac{r}{6}\left[\left(\frac{A_{11}}{(d_i+\Delta d)^2}\right)^{th} + \left(\frac{A_{12}}{(d_j+\Delta w_{j,t})^2}\right)^{sd} \right], \quad (3)$$

where $F-C$ refers to flat-curved surface interaction between two grains, and r denotes a parameter for the grain size, respectively.

Similar to Figure 1, Figure 2 shows the schematic of typical curved-curved surface interaction. Concerning Figure 2, the net interfacial stress function for curved-curved surface interaction as a function of temperature and time can be described by

$$\sigma_{\mathrm{j},t(C-C)}^{net} = -\left(\frac{1}{6}\right)\left(\frac{r_1 r_2}{r_1+r_2}\right)\left[\left(\frac{A_{11}}{(d_i+\Delta d)^2}\right)^{th} + \left(\frac{A_{12}}{(d_j+\Delta w_{j,t})^2}\right)^{sd} \right]. \quad (4)$$

where $C-C$ refers to curved-curved surface interaction between two grains.

In every case, $r >> d_j$ or d_i. For optimum results, d_j or $d_i << r/100$. Here, r is taken to be a function of the side

length of the interacting grains in the film structure. r is estimated from the value of d_j or d_i of the material understudied.

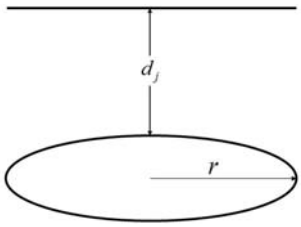

Figure 1. *Schematic showing flat-curved surface interaction. r denotes a parameter for the grain size.*

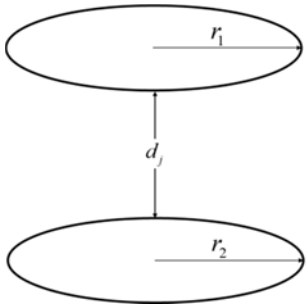

Figure 2. *Schematic showing curved-curved surface interaction. r denotes a parameter for the grain size.*

3. Results and Discussion

Specific results for the interfacial stress based on the interactions of grains at the interface were calculated by the DEM approach described by equations (1), (3), and (4) and compared with that computed by the closed-form solution model described by Cheon, J. H., *et al*., as follows [24]

$$\sigma_j = E_{eq.}(\alpha_i - \alpha_{i+1})\Delta T\,, \tag{5}$$

$E_{eq.}$ is the equivalent Young's modulus of the film, it is replaced by $E_i/1\text{-}v_i$ for planar geometry, v is the Poisson ratio, α is the coefficient of thermal expansion, and T is the temperature.

Also, specific computed results by the DEM approach was compared with that measured by X-ray Diffraction ($\sin^2\varphi$ method) for films processed by pulsed laser deposition (PLD) technique described by Cheon, J. H., *et al*. and Xiong, J., *et al*., [25, 26]

$$\varepsilon_{res.} = \frac{\Delta d}{d} = \left(\frac{d_\varphi - d_\perp}{d_\perp}\right) = \sigma_{\phi_x}\frac{(1-v)}{E}\sin^2\varphi\,, \tag{6}$$

where $\varepsilon_{res.}$ is the residual strain in the films, d_φ and $d_\perp$ are measured lattice constant of films at angles φ and 0° to the third principal stress (σ_3) in crystal X-ray diffraction (XRD) files and σ_{ϕ_x} is the residual stress acting on the surface of the film in the direction of a particular angle ϕ_x from the first principal stress (σ_1).

3.1. The Interfacial Stress in Yttrium Barium Copper Oxide (YBCO) Films Deposited on $LaAlO_3$ Substrate

With the experiment conducted by Cheon *et al*., [25], in this study, the author investigated the residual interfacial stress in yttrium barium copper oxide (YBCO) film deposited on Lanthanum aluminum oxide ($LaAlO_3$) substrate by the PLD technique. The specimen measured 1.5 cm × 1.2 (length × width). Also, the deposition temperature of the YBCO was 780°C. Other physical/mechanical properties of the specimen are given in Table 1 [25, 27]. Next, the computed Hamaker coefficient (based on equation (2)) for the YBCO crystal and its interfacial is 12×10^{-20} J (i.e., $A_{11} = A_{12}$). These values were strictly implemented on the corresponding equations to obtain the specific results of residual interfacial stress in the YBCO film for two interacting grains with similar and different surface morphologies described by equations (1), (3), and (4), accordingly.

Table 1. *Physical constants for the materials of yttrium barium copper oxide (YBCO), and Lanthanum aluminum oxide ($LaAlO_3$). h is thickness, E is Young's modulus, v is the Poisson ratio, ρ is the mass density, CTE is the coefficient of thermal expansion and d_i denotes a standard lattice constant between two same material bonded surfaces.*

Parameters	h (μm)	E (GPa)	v	ρ (g/cm^3)	CTE (10^{-6}K^{-1})	d_i (nm)
YBCO	0.5	157.0	0.30	6.30	13.4	0.3850
$LaAlO_3$	200.0	500.0	0.30	6.52	10.0	0.3792

3.1.1. Intrinsic Interfacial Stress Function in the YBCO Films for Unit Grain Size ($r = 1$ Unit)

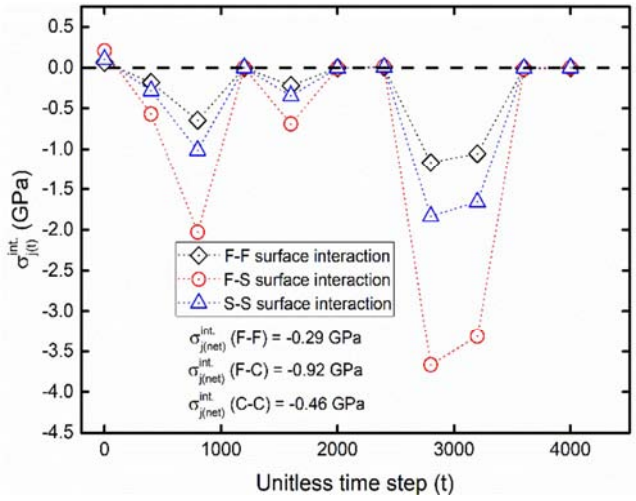

Figure 3. *Intrinsic interfacial stress function, $\sigma^{int.}_{j,t}$ in the YBCO films deposited on $LaAlO_3$ substrate in time. F-F denotes two interacting grains with flat-flat surfaces, F-C denotes two interacting grains with flat-curved surfaces, and C-C denotes two interacting grains with curved-curved surfaces.*

As noted earlier, the dependence of the residual interfacial stress on the power of the lattice constant (d_j) of the two interacting grains suggests that it would change with the change in the surface morphology of the interacting grains. Also, the DEM equations describing the net interfacial

residual stress of the given surface morphology of the interacting grains contain a different combination of the essential parameters, as indicated by equations (1), (3), and (4). These further suggest a change in the residual interfacial stress with the change in the surface morphology of the interacting grains.

Figure 3 shows the interfacial residual stress function, $\sigma_{j,t}^{int.}$ in the YBCO films deposited on $LaAlO_3$ substrate due to the dynamics of the thin-film structure as a function of time. As noted earlier, the DEM approach results give the C-T-C residual stress-evolution in the thin-film structure as a function of time, as indicated in Figure 3. Here and after that, the positive values in the Figures (i.e., the points above the horizontal dashed lines) denote the interfacial tensile residual stress. In contrast, the negative values in Figures (i.e., the points below the horizontal dashed lines) denote the interfacial compressive residual stress. As shown in Figure 3, the F-F surface interaction indicates the lowest net interfacial residual stress of -0.29 GPa.

In contrast, the F-C surface interaction indicates the highest net interfacial stress of -0.92 GPa. Still, in Figure 3, the C-C surface interaction suffers an intermediate net interfacial residual stress of -0.46 GPa. The author believed the active interfacial residual stress in the YBCO films is influenced by the active contact surface area of the two interacting grains. Typically, the contact pressure between the two grains is force per unit area. Thus, for the first case (i.e., F-F surface interaction), the active contact surface of the two interacting grains is comparatively higher. A comparatively higher effective contact surface of the two interacting grains would give relatively lower net interfacial residual stress in the YBCO films, as indicated by the F-F surface interactions in Figure 3. For the second case (i.e., F-C surface interaction), the active contact surface of the two interacting grains is comparatively lower. This would give relatively higher net interfacial residual stress in the YBCO films, as indicated by the F-C surface interaction in Figure 3. The active contact surface of the C-C surface interaction is similar to that of the F-F surface interaction because the ratio of the interacting surface of the first to the second grain is 1:1. However, the active contact surface of the F-F surface interaction is higher compared with the C-C surface interaction. Hence, the C-C surface interaction suffers higher interfacial residual stress of -0.46 GPa compared with the F-F surface interaction, which is -0.29 GPa.

This finding agrees with the explanations of valuable experiments in the literature [28, 29]. A recent critical validation and comparison of the three conventional methods; the Wafer Curvature Method (WCM), X-Ray Diffraction Method (XRD), and Focused Ion Beam Method (FIBM) for measuring residual stress in thin-films showed an excellent agreement between the FIBM and cross-sectional nano-diffraction XRDM [10]. On the other hand, the WCM showed slightly lower stress values compared with the FIBM. The observed difference between the stress values measured by the WCM and FIBM was attributed to the comparatively different gauge volume of their information source. The FIBM experiments acquire information from a small gauge volume (a few μm^3 of the specimen).

On the other hand, the WCM acquires information from a large volume (usually the entire volume of the specimen). Also, the WCM includes stress relaxation phenomena concerning the presence of micro-cracks and micro-droplet over the entire surface. Therefore, with regards to these results, it would infer that the surface morphology of the interacting grains affects the net intrinsic residual stress in the YBCO films significantly.

3.1.2. Interfacial Thermal Stress $\sigma_{j(net)}^{th.}$ in the YBCO Films for Unit Grain Size ($r = 1$ Unit)

Figure 4 shows the net interfacial thermal stress in the YBCO films due to its thermal mismatch with the $LaAlO_3$. As shown in Figure 4, YBCO films suffer interfacial residual tensile stress. The YBCO films suffer tensile stress due to thermal mismatch between the $LaAlO_3$ because the coefficient of thermal expansion of the YBCO is higher compared with that of the $LaAlO_3$, as given in Table 1. Still, in Figure 4, it could be observed that the interacting grains with F-S surfaces suffer the highest interfacial tensile thermal stress. In contrast, those with F-F surface interactions suffer the lowest interfacial tensile thermal stress.

Concerning the thermal mismatch phenomenon, the author could not ascertain the exact cause of the different interfacial tensile thermal stress exhibited by the interacting grains with different morphology. However, the author are hypothesizing; this could be due to different heat flux through the active contact surface of the interacting grains. There is a primary understanding that a large surface allows more flow of heat, conducting electrons compared with a small surface. If that is the case, it implies that grains with a comparably sizeable active contact surface would have more stress relaxation, thereby lowering the net interfacial thermal stress in the F-F surface interactions, as indicated in Figure 4.

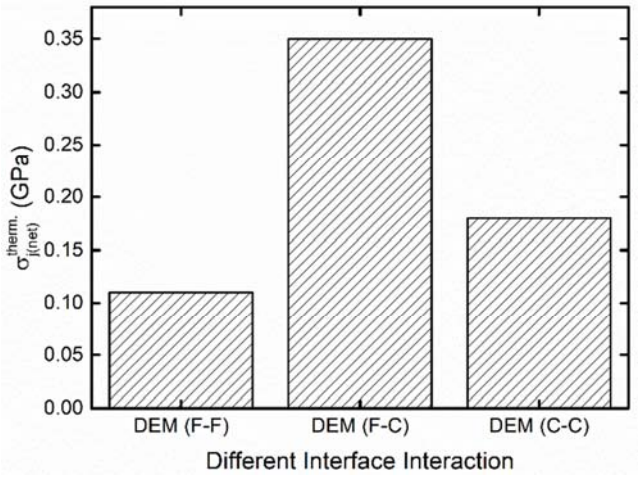

Figure 4. *Net interfacial thermal stress in the YBCO films deposited on $LaAlO_3$ substrate. F-F denotes two interacting grains with flat-flat surfaces, F-C denotes two interacting grains with flat-curved surfaces, and C-C denotes two interacting grains with curved-curved surfaces.*

3.1.3. Overall Net Residual Interfacial Stress (i.e., $\sigma_j^{\text{net}} = \sigma_{\text{j}(net)}^{\text{th.}} + \sigma_{\text{j}(net)}^{sd.}$) in the YBCO Films

As stated earlier, in the analysis of the DEM approach, the stress-inducing mechanisms in a thin-film structure are due to the strong effects of the thermal mismatch, and the structural dynamics of the interacting grains. Therefore, the overall net residual interfacial stress in the YBCO described by equations (1), (3), and (4) is shown in Figure 5. Also, shown in Figure 5 is the residual interfacial stress in the YBCO films computed by the Closed-form solution (CFS) model for comparison. As indicated in Figure 5, the overall net interfacial stress in the YBCO films is compressive in all scenarios. Also, in Figure 5, on the DEM approach, the YBCO grains with F-C surface interaction suffer the highest interfacial stress of -0.56 GPa.

In contrast, those with F-F surface interaction suffer the lowest interfacial stress of -0.18 GPa. Still, in Figure 5, on the CFS model, the strip interfacial stress in the YBCO films is lower compared with that of the biaxial film. On the comparison of the two models, on the one hand, the result obtained by the DEM approach for the YBCO grains with F-C surface interaction agrees well with the result obtained by the CFS model for the YBCO grains with biaxial (planar) geometry as shown in Figure 5. In this case, the absolute difference between the results obtained by the two models is only 0.02 GPa.

On the other hand, taking the average of the net interfacial residual stress in the YBCO films by the CFS model gives the interfacial stress of -0.49 GPa. Similarly, taking the mean of the net interfacial stress in the YBCO films by the DEM approach gives the interfacial stress of -0.34 GPa. In this case, the absolute difference between the results obtained by the two models is 0.15 GPa.

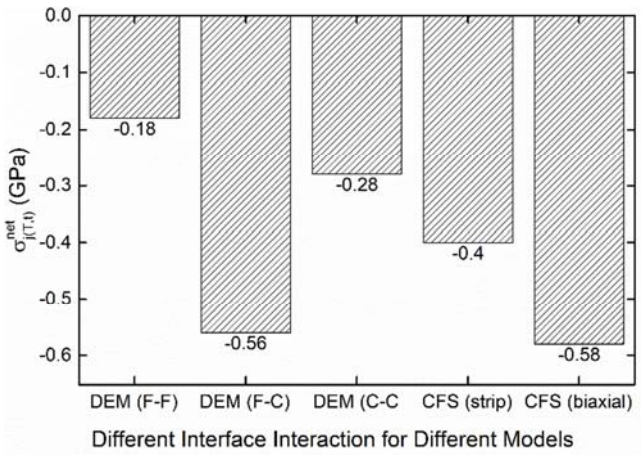

Figure 5. *Overall net interfacial stress (i.e., $\sigma_f^{\text{net}} = \sigma_{f(net)}^{\text{th.}} + \sigma_{f(net)}^{sd.}$) in the YBCO films deposited on $LaAlO_3$ substrate for unit grain size ($r = 1$ unit) computed by different models (the DEM approach and Closed-form solution method (CFS)). F-F denotes two interacting grains with flat-flat surfaces, F-C denotes two interacting grains with flat-curved surfaces, and C-C denotes two interacting grains with curved-curved surfaces.*

Figure 6 shows the net interfacial stress in the YBCO films measured by the XRD method and those computed by the DEM approach for comparison. As shown in Figure 6, the measured net interfacial stress in YBCO films is 0.178 ± 0.053 GPa. Still, in Figure 6, the computed result of the net interfacial stress by the DEM approach for the YBCO interacting grains with C-C surfaces is 0.18 GPa. In contrast, those with F-C surfaces are 0.35 GPa. Also, the computed result of the net interfacial stress by the DEM approach for the YBCO interacting grains with F-F surfaces is 0.11 GPa, as indicated in Figure 6.

Concerning the YBCO interacting grains with the given interacting surfaces, the grains with C-C surfaces agree excellently well with the measured XRD value. On the other hand, the interacting grains with the F-C and F-F surfaces are significantly higher and lower, respectively, compared with the XRD measured value. In this regard, it is known that the energy of ions due to the local heating from the X-ray beam might alter the original internal stresses of the sample, thereby influencing its measured net interfacial residual stress [25, 26]. In this study, as indicated in our earlier study, the author's assumption of the initial Eigenfunction (W_0) equal to $\geq 10^{-9}$ m is equivalent to the PLD technique [14]. This initial Eigenfunction is a reasonable estimate of the PLD technique.

Thus, one could rely on the value of the net interfacial stress obtained by the DEM approach for the YBCO interacting grains with C-S surfaces, which agrees well with the result of the measured value by the XRD method. Better still, one could rely on the mean value of the net interfacial stress obtained by the DEM approach, which is approximate 0.21 GPa. This is only 0.02 GPa lower compared with the upper value of the measured value by the XRD method, which is approximate 0.23 GPa. Thus, the result of the DEM approach agrees reasonably well with the XRD method.

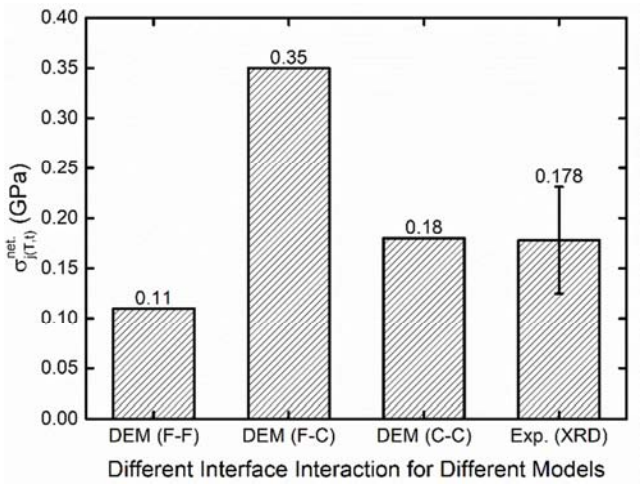

Figure 6. *Comparison of the net interfacial tensile stress of two interacting grains with similar and different surface interactions obtained by a different method (the DEM approach and X-ray diffraction method (XRD) methods).*

3.2. Impact of the Grain Size on the Interfacial Stress in the YBCO Films Deposited on $LaAlO_3$ Substrate

The presence of the grain size parameter (r) as indicated in equations (3) and (4) suggests that the grain size would affect the interfacial stress-evolution in the thin-film structure. Figure 7 shows the effect of the grain size parameter on the interfacial intrinsic stress function in the YBCO films

deposited on $LaAlO_3$ for the interacting grains with F-C surfaces. As shown in Figure 7, it can be observed that the interfacial intrinsic stress in the YBCO films increases with the increase in the grain size parameter.

On the one hand, the author believes the increase of the intrinsic interfacial with the increase in the grain size is based on the phenomenon of the active contact surface of the two interacting grains explained earlier in sections 3.1.1 and 3.1.2. Thus, the grain size affects the interfacial stress evolution in the YBCO films significantly.

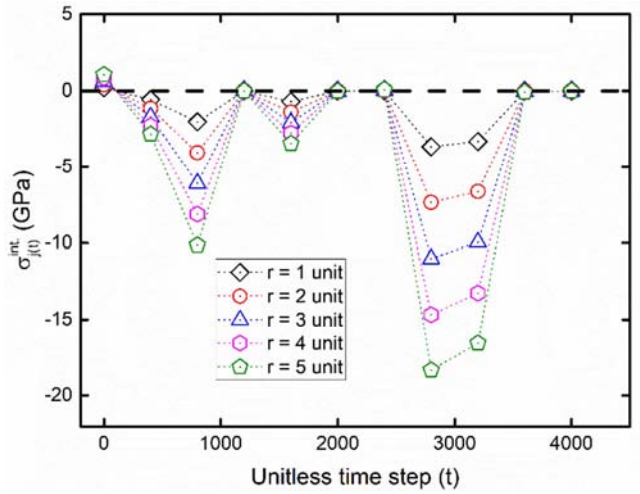

Figure 7. *Effect of the grain size on the interfacial intrinsic stress in the YBCO films for two interacting grains with the F-C surfaces in time.*

4. Summary

In summary, the author extended the displacement-energy model (DEM) approach to determine the interfacial stress in a multilayered film structure based on the interactions of the grains at the interface. In this approach, the stress-inducing mechanisms in a thin-film structure are due to the strong effects of the thermal mismatch and structural dynamics of the interacting grains experienced during deposition processes. The stress-inducing mechanisms are related to the displacement-energy phenomenon in the structure caused by the kinetic and thermal energy of the deposited films and deposition flux gas. In contrast, the stress evolution in the deposited films is determined from the change of lattice constant of the interacting grains as a function of temperature and time caused by the different coefficients of thermal expansion and eigenstates of the materials.

Here, the author considered grains that consist of cubic, pyramid, pyramid frustum, and spherical morphology. Hence, the interacting surfaces included flat-flat surface interaction, flat-curved surface interaction, and curved-curved surface interaction. Accordingly, the author developed specific models for interacting grains with the considered interacting surfaces (i.e., curved surfaces interaction). These models were implemented on YBCO films deposited on $LaAlO_3$ substrate by the PLD technique. Also, the results obtained by the DEM approach were compared with those obtained by the closed-form solution (CFS) and x-ray diffraction (XRD) methods described elsewhere.

The computed results show that the surface morphology, and size of the interacting grains affect the net interfacial stress in the YBCO films significantly. On the comparison of the two models (i.e., DEM and CFS), on the one hand, the result obtained by the DEM approach for the YBCO grains with F-C surface interaction agrees well with the result obtained by the CFS model for the YBCO grains with biaxial (planar) geometry. The result obtained by the DEM approach for the YBCO grains with F-C surface interaction is -0.56 GPa. Similarly, the result obtained by the CFS model for the YBCO grains with biaxial (planar) geometry is -0.58 GPa. On the other hand, taking the average of the net interfacial stress in the YBCO films by the CFS model (i.e., for strip and biaxial geometry) gives the compressive stress of -0.49 GPa.

However, taking the mean of the net interfacial residual stress in the YBCO films by the DEM approach gives the compressive stress of -0.34 GPa. In this case, there is a significant difference between the two models. Also, on the comparison of the DEM approach with the XRD method, on the one hand, the DEM result obtained for the interacting grains with C-C surfaces agrees well with the measured value of the XRD method. The interfacial stress in the YBCO film obtained by the DEM for the interacting grains with C-C surfaces is 0.18 GPa. Similarly, that measured by the XRD method is 0.178 ± 0.053 GPa.

On the other hand, the mean interfacial stress obtained by the DEM approach for all considered grains interacting surfaces also agrees well with the measured upper value of the XRD method. The mean interfacial stress obtained by the DEM approach for all considered grains interacting surfaces is 0.21 GPa. Similarly, the measured upper value of the XRD method is 0.23 GPa. The author believes an excellent agreement between the DEM approach and the XRD method is because the author's assumption of the initial Eigenfunction (W_0) equal to 1×10^{-9} m is equivalent to the PLD technique used in the XRD method.

Although in our earlier studies, as well as the current study, the DEM approach showed high fidelity in interpreting the damage and interfacial stress evolutions in multilayer thin-film structures, the author advocate for more valuable studies on these critical findings of the interfacial stress based on the interactions of the grains presented in this study. It would be necessary to evaluate grains with flat-cylindrical, spherical-cylindrical, and cylindrical-cylindrical interaction surfaces.

Also, experiments to determine the actual combination of the morphologies of the interacting surfaces of specific crystals are essential. In particular, the author believes the DEM solution approach can help relieve researchers from some costly experiments involved in the mechanical characterization of multilayer film structures. Moreover, the author believes that this understanding of the dependence of interfacial stress on the morphology and size of interacting grains revealed in this study would be essential in the mechanical characterization of several Multilayer Engineering Materials, including composites for various applications,

which often consist of grains with different morphology and size.

Funding

No funding is received for this work.

References

[1] Mbam, S. O., Nwonu, S. E., Orelaja, O. A., Nwigwe, U. S., Gou, X-F. Thin-film coating; historical evolution, conventional deposition technologies, stress-state micro/nano-level measurement/models and prospects projection: a critical review. *Materials Research Express*, 6 (12) 122001, (2019).

[2] Ogata, M., Miyazaki, Y., Hasegawa, H., Sasakawa, T., Nagashima, K. Basic study of HTS magnet using 2G wires for maglev train. *Physica C: Superconductivity and its Applications*, 470, 1782-6, (2010).

[3] Bernstein, P., Noudem, J. Superconducting magnetic levitation: principle, materials, physics, and models. *Superconductor Science and Technology*, 33, 033001, (2020).

[4] Ikeda, R., Ota, S., Aiba, M., Yoda, H., Watanabe, K. Insulation Diagnosis with a Focus on Partial Discharge of the Propulsion Coils of the Superconducting Maglev. *Quarterly Report of RTRI*, 61, 66-71, (2020).

[5] Dong, F., Huang, Z., Xu, X., Wang, M., Teng, X., Hao, L., *et al*. Method and Process of Mechanical Evaluation of a 2G HTS Magnet System for Maglev Applications. *IEEE Transactions on Applied Superconductivity,* 30, 1-5, (2020).

[6] Lee, T. D., Ebong, A. U. A review of thin-film solar cell technologies and challenges. *Renewable and Sustainable Energy Reviews,* 70, 1286-97, (2017).

[7] Chopra, K, A Technical Review on the Thin-Films Coatings for Enhancing the Efficiency of the Photo-Voltaic Cells for Solar Energy Applications. *Invertis Journal of Renewable Energy*, 2, 199-207, (2012).

[8] Xue, D-J., Liu, S-C., Dai, C-M., Chen, S., He, C., Zhao, L., *et al*. GeSe thin-film solar cells fabricated by self-regulated rapid thermal sublimation. *Journal of the American Chemical Society*, 139, 958-65, (2017).

[9] Jeong, E. G., Lim, M. S., Choi, K. C. *P-129: Zero-Stress Thin-film Encapsulation Method for Increasing the Intrinsic Stability of Flexible OLEDs. SID Symposium Digest of Technical Papers*, Wiley Online Library, 1746-9, (2017).

[10] Abadias, G., Chason, E., Keckes, J., Sebastiani, M., Thompson, G. B., Barthel, E., *et al*. Stress in thin films and coatings: Current status, challenges, and prospects. *Journal of Vacuum Science & Technology A: Vacuum, Surfaces, and Films*, 36, 020801, (2018).

[11] Korzeniewska, E., Szczęsny, A. Parasitic parameters of thin-film structures created on flexible substrates in PVD process. *Microelectronic Engineering*, 193, 62-4, (2018).

[12] Xia, W., Song, J., Hsu, D. D., Keten, S. Understanding the interfacial mechanical response of nanoscale polymer thin films via nanoindentation. *Macromolecules*, 49, 3810-7, (2016).

[13] Li, Z-X., Cao, J-J., Gou, X-F., Wang, T-G., Xue, F. Uncovering a new quasi-2D CuO_2 plane between the $YBa_2Cu_3O_7$ and CeO_2 buffer layer of coated conductors. *Applied Surface Science*, 427, 169-73, (2018).

[14] Mbam, S. O., Gou, X-F. An analytical method for predicting the net (thermal plus intrinsic) residual stresses in multilayered yttrium barium copper oxide coated conductors. *Materials Research Express*, 6, 096002, (2019).

[15] Sugino, C., Ruzzene, M., Erturk, A. An analytical framework for locally resonant piezoelectric metamaterial plates. *International Journal of Solids and Structures*, 182, 281-94, (2020).

[16] Cheikh, I. B., Parry, G., Dalmas, D., Estevez, R., Marthelot, J. Analysis of the multi-cracking mechanism of brittle thin films on elastic-plastic substrates. *International Journal of Solids and Structures*, 180, 176-88, (2019).

[17] Mikula, J., Joshi, S. P., Tay, T-E., Ahluwalia, R., Quek, S. S. A phase-field model of grain boundary migration and grain rotation under elastoplastic anisotropies. *International Journal of Solids and Structures*, 178, 1-18, (2019).

[18] Mbam, S. O., Jiang, Z-F., Gou, X-F. A displacement-energy model of studying the delaminating behavior of multi-layer REBCO coated conductor tapes. *Physica C: Superconductivity and its Applications*, 560, 10-8, (2019).

[19] Chason, E., Shin, J., Hearne, S., Freund, L. Kinetic model for dependence of thin-film stress on growth rate, temperature, and microstructure. *Journal of Applied Physics*, 111, 083520, (2012).

[20] Chason, E., Karlson, M., Colin, J., Magnfält, D., Sarakinos, K., Abadias, G. A kinetic model for stress generation in thin films grown from energetic vapor fluxes. *Journal of Applied Physics*, 119, 145307, (2016).

[21] Mbam, S. O., Gou, X-F. Inspection of Fabrication Defects in REBCO Coated Conductors from Various Industrial Manufacturers under Similar Fabrication Conditions using the DEM Approach. *Physica C: Superconductivity and its Applications*, 1353664, (2020).

[22] Mbam, S. O., Gou, X-F. Fabrication stacking faults and its influence on the delamination behavior of SuperPower (SCS4050®) tapes. *Engineering Failure Analysis*, 104609, (2020).

[23] Mbam, S. O., Gou, X-F. Uncovering and elimination of the natural separation of interacting molecules of standard REBCO crystals, a panacea for improvement of its delamination strength. *Engineering Failure Analysis*, 107, 104196, (2020).

[24] Hsueh, C., Paranthaman, M. Analytical modeling of residual stresses in multilayered superconductor systems. *Journal of Materials Science*, 43, 6223-32, (2008).

[25] Cheon, J. H., Shankar, P. S, Singh, J. P. Influence of processing methods on residual stress evolution in coated conductors. *Superconductor Science and Technology*, 18, 142-6, (2005).

[26] Xiong, J., Qin, W., Cui, X., Tao, B., Tang, J., Li, Y. Effect of processing conditions and methods on residual stress in CeO_2 buffer layers and YBCO superconducting films. Physica C: Superconductivity and its Application, 442, 124-8, (2006).

[27] Xu, Y., Shi, D. A review of coated conductor development. *Tsinghua science and technology*, 8, 342-69, (2003).

[28] Ghidelli, M., Sebastiani, M., Collet, C., Guillemet, R. Determination of the elastic moduli and residual stresses of freestanding Au-TiW bilayer thin films by nanoindentation. *Materials & Design*, 106, 436-45, (2016).

[29] Korsunsky, A. M., Sebastiani, M., Bemporad, E. Residual stress evaluation at the micrometer scale: Analysis of thin coatings by FIB milling and digital image correlation. *Surface and Coatings Technology*, 205, 2393-403, (2010).